Differential pumping for kHz operation of a Laser Wakefield accelerator based on a continuously flowing Hydrogen gas jet

Joséphine Monzac, Slava Smartsev, Julius Huijts, Lucas Rovige, Igor Andriyash, Aline Vernier, Vidmantas Tomkus, Valdas Girdauskas, Gediminas Raciukaitis, Miglė Mackevičiūtė, et al.

Differential pumping for kHz operation of a Laser Wakefield accelerator based on a continuously flowing Hydrogen gas jet

J. Monzac,[1,*] S. Smartsev,[1] J. Huijts,[1] L. Rovige,[1] I.A. Andriyash,[1] A. Vernier,[1] V. Tomkus,[2] V. Girdauskas,[2,3] G. Raciukaitis,[2] M. Mackevičiūtė,[2] V. Stankevic,[2] A. Cavagna,[1] J. Kaur,[1] A. Kalouguine,[1] R. Lopez-Martens,[1] and J. Faure[1]

[1] *LOA, CNRS, École Polytechnique, ENSTA Paris, Institut Polytechnique de Paris, Palaiseau, France*

[2] *Center for Physical Sciences and Technology, Savanoriu Ave. 231, LT-02300, Vilnius, Lithuania*

[3] *Vytautas Magnus University, K.Donelaicio St. 58. LT-44248, Kaunas, Lithuania*

Laser-Wakefield Accelerators (LWFA) running at kHz repetition rates hold great potential for applications. They typically operate with low-energy, highly compressed laser pulses focused in high-pressure gas targets. Experiments have shown that the best-quality electron beams are achieved using Hydrogen gas targets. However, continuous operation with Hydrogen requires a dedicated pumping system. This work presents the design of a differential pumping system, enabling, for the first time, continuous operation of our kHz LWFA using a high-pressure Hydrogen gas jet. The system successfully maintained a pressure below 3×10^{-4} mbar, even with a free-flowing gas jet operating at 140 bar backing pressure. Numerical fluid dynamics and optical simulations were used to guide and validate the system's design.

I. INTRODUCTION

Laser wakefield acceleration (LWFA) is a process that enables the generation and acceleration of electron beams to relativistic energies over very short distances [1]. An ultrashort laser pulse is focused into a plasma, and drives a large density amplitude plasma wave in which plasma electrons can be trapped and accelerated. Since the plasma is already ionized, the electric field of the plasma wave is not subject to the breakdown limit that exists in conventional radiofrequency (RF) cavities. Thus the accelerating field can reach amplitudes up to 4 orders of magnitude higher than in conventional RF cavities: acceleration can occur over much shorter distances, paving the way for compact accelerators.

In LWFA, the laser first propagates through a vacuum before being focused into a plasma, where the acceleration process occurs. The plasma is generated as the laser ionizes the gas supplied by the target system. Various types of gas targets can be used in LWFA. Each type is designed to balance the required plasma density while minimizing gas leakage, which increases the pressure in the vacuum chamber where the laser propagates. Here are the most commonly used target systems: (i) gas jets: a supersonic gas flow expands from a nozzle into the vacuum chamber [2, 3], (ii) gas cells: provide an enclosed gas interaction volume where the laser propagates between two apertures at the entrance and exit of the cell [4]. These apertures must be small enough to minimize gas leakage in the main chamber, but large enough to avoid ablation from the laser which would in turn negatively affect the laser performance. In order to mitigate the leaks, the gas cells operate at lower gas pressures, resulting in lower plasma densities compared to gas jets. Additionally, some gas cells utilize differential pumping, where the gas is removed from the cell simultaneously as it is introduced [5, 6]. A last commonly used target system is the capillary discharge target, where the plasma is generated via a high-voltage discharge. There, the laser propagates through the guided mode of the plasma channel formed during plasma expansion and interaction with the capillary walls [7]. This approach is relevant when long acceleration distances are needed (in the range of 1 cm), but it remains sensitive as the entrance capillary aperture can be damaged by high-intensity lasers. It is worth noticing that similar target systems are also being employed in the field of nuclear physics. Notably, some of their experiments make use of gas jets combined with differential pumping techniques, though these systems generally operate at much lower densities than those in the present study [8–11]. Early-stage designs and implementations of such differential pumping systems have been explored in the frame of LWFA [12].

Advances in laser technology, along with the development of the target systems, have led to tremendous progress in the laser-plasma accelerator performances. Today, LWFA driven by 100 TW to PW scale laser systems can produce electron beams with energies ranging from 100 MeV to GeV over a few centimeters [13–18]. To date, the highest energy ever reached is 8 GeV using plasma discharge technology [19].

While pushing the energy frontier is important for high-energy physics, another line of research focuses on the development of high repetition-rate (100 Hz - 1 kHz) LWFAs, which holds significant potential for enhancing stability and enabling the acquisition of large datasets, essential for robust statistical analysis. Until recently, kHz laser systems were restricted to a few millijoules per pulse. To fulfill the conditions for laser-wakefield acceleration using such energies, it is necessary to tightly

* josephine.monzac@ensta-paris.fr

focus and strongly compress the laser pulse, and to work with very high electron densities in the plasma on the order of $n_e \sim 10^{20}\,\mathrm{cm}^{-3}$ [20–23]. The high electron density imposes the use of free-flowing gas jets, which can provide such densities and handle kHz operation to refresh the target. The continuous operation of LWFA at 1 kHz has been demonstrated using Nitrogen [21, 24]. However, recent experimental work shows that using light gases such as Hydrogen is beneficial to LWFA and that higher electron energy and better spatial beam properties can be reached [25].

Regarding vacuum conditions, utilizing a nitrogen plasma is convenient: each N_2 molecule provides 10 electrons, enabling a backing pressure of only 20 to 30 bar in the gas jets to achieve the required plasma density. Additionally, heavy gases like nitrogen are easier to pump than light gases [26, 27]. However, ionization effects can significantly distort the laser pulse in N_2 as different levels are ionizes at different positions within the laser pulse, causing a decrease in accelerator performance. To counter this, utilizing a light gas such as hydrogen is necessary [28]. So far, kHz-scale experiments using an H_2 plasma have been limited to burst mode operation as pumping H_2 poses significant challenges [23, 25]. When a free-flowing gas jet of H_2 is used at high pressure, it results in considerable gas loading in the vacuum chamber where the experiment is conducted. This phenomenon was observed by Salehi et al. [25], who reported a rapid pressure increase in the main chamber, rising from 2.6×10^{-2} mbar to 2.0×10^{-1} mbar in just 1 second when using a free-flowing gas jet with a $\sim 150\,\mu$m FWHM aperture and a backing pressure of ~ 30 bar. They operated in burst mode and avoided gas loading in their experiments.

This paper describes the design, implementation, and testing of a differential pumping scheme for a continuously flowing gas nozzle used in a kHz laser-plasma accelerator. It is structured as follows: Section II introduces the physical principles underpinning the design of the differential pumping system, as well as a thorough analysis demonstrating its necessity and effectiveness. In Section III, we conduct fluid simulations and laser propagation simulations to verify the absence of laser distortion caused by gas stagnation in the small chamber. Section IV details the integration of this apparatus into our experimental setup and presents the results obtained through the implementation of the differential pumping system. Finally, Section V provides a summary of the findings and concludes the paper.

II. DIFFERENTIAL PUMPING FOR GAS JETS AND HIGH PRESSURE LIGHT GASES

The optimal plasma density and length for a laser-plasma accelerator depend on the physical properties of the laser pulse.In the case of a few mJ, few fs pulse, the plasma density should typically be $n_e \sim 10^{19} - 10^{20}\,\mathrm{cm}^{-3}$ and the plasma length $L = 100 - 200\,\mu$m. To reach such plasma parameters, we use supersonic cylindrical gas nozzles and backing pressures ranging from a few tens of bar to about 150 bar. A cross-section diagram of the gas jet is shown in Figure 1b. In the following, we will refer to the gas nozzle parameters as follows: the diameter of the nozzle throat and nozzle opening are respectively written D^* and D and the corresponding throat and opening surfaces are A^* and A, where we simply have $A = \pi D^2/4$. For example, a 60/180 gas nozzle has $D^* = 60\,\mu$m, $D = 180\,\mu$m, and provides the right plasma length and molecular density $n_{N_2} \sim 10^{19}\,\mathrm{cm}^{-3}$ when using N_2 gas with pressure $P_{back} = 30$ bar backing pressure (see Figure 1a). The laser pulse is intense enough to ionize Nitrogen atoms to N^{5+}, so that each N_2 molecule releases 10 electrons, leading to the required plasma electron density of $n_e \sim 10^{20}\,\mathrm{cm}^{-3}$.

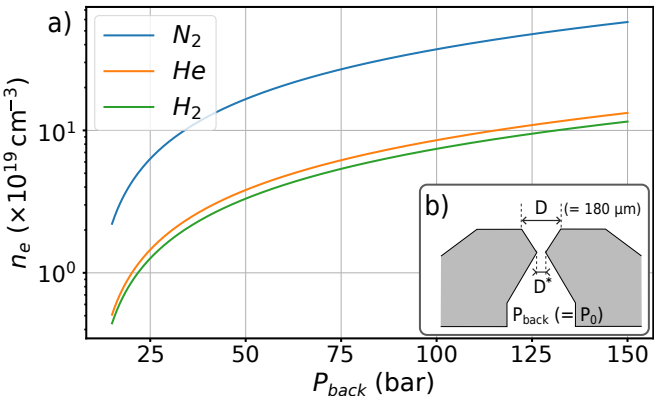

Figure 1. a) Electronic density n_e of the plasma as a function of the backing pressure in the gas jet and the nature of the gas. b) Cross section of the supersonic gas jet, D^* and D are respectively the diameter of the nozzle throat and nozzle opening.

A. Differential pumping use in high repetition rate LWFA

The pumping system is designed so that the residual equilibrium pressure in the interaction chamber, $P_{eq}^{(1)}$ stays sufficiently low and does not affect laser propagation. We set this limit empirically to $P_{eq}^{(1)} < 10^{-2}$ mbar since above this value, turbo-molecular pumps become inoperative, overheat, and the system diverges. The residual pressure at equilibrium $P_{eq}^{(1)}$ in the chamber can be estimated knowing the pumping speed R_{eff}[l/s] and the gas leak rate due to the gas jet Q[mbar · l/s] by simply writing that:

$$P_{eq}^{(1)}[\mathrm{mbar}] = Q[\mathrm{mbar}\cdot\mathrm{l/s}] \;/\; R_{eff}[\mathrm{l/s}] \qquad (1)$$

This allows to easily estimate the gas leak rate in our experiment. Typically, in Nitrogen, using a nozzle with

$D^* = 50\,\mu$m and a backing pressure of $P_{back} = 20$ bar, we measure $P_{eq}^{(1)} = 3 \times 10^{-3}$ mbar. Knowing that the pumping speed of our turbo-molecular pump is $R_{eff} = 4000$ l/s for Nitrogen, we obtain that the gas leak is $Q = 12$ mbar.l/s.

Let us now calculate what happens if one uses H_2 instead of Nitrogen. We assume complete ionization: each H_2 molecule now releases 2 electrons instead of 10 in N_2. In addition, we use a 1D isentropic expansion model for compressible gas flows to extrapolate the molecular density in H_2. The molecular density in the flow, n_{mol}, can be expressed according to the Boltzmann constant k_B, the Mach number M_{Mach} and the initial pressure and temperature, P_0, T_0 in the reservoir [29].

$$n_{mol} = \frac{P_0}{k_B T_0}\left(1 + \frac{\gamma - 1}{2} M_{Mach}^2\right)^{-\frac{1}{\gamma - 1}} \tag{2}$$

The coefficient $\gamma = c_p/c_v$ is the ratio of specific heat at constant pressure c_p over the specific heat at constant volume c_v. For perfect diatomic gases such as N_2 and H_2, $\gamma = 7/5$, whereas for a perfect monoatomic gas, such as He, $\gamma = 5/3$. For our gas jet, where $M_{Mach} \gtrsim 3$, with $P_0 = 20$ bar and $T_0 = 300$ K, we obtain the same molecular density at the exit of the nozzle $n_{mol} = 4.3 \times 10^{18}$ cm^{-3} for N_2 and H_2. The resulting electronic density is $n_e = 4.3 \times 10^{19}$ cm^{-3} for N_2 and $n_e = 8.6 \times 10^{18}$ cm^{-3} for H_2. The final electronic density as a function of the backing pressure for different gases is shown in Figure 1a. Using H_2 the backing pressure should be increased by a factor of 5 to reach the same electronic density as in N_2, i.e. $P_0 = 100$ bar, which means a 5-fold increase in the gas flow. In addition, the leak rate depends on the mass of the molecule as $Q \propto \sqrt{M}$ which is another aggravating factor for the case of H_2 (see next section). Thus, for the same final electron plasma density, the leak rates in H_2 and N_2 are related as:

$$Q_{H_2} = 5 Q_{N_2}\left(\frac{M_{N_2}}{M_{H_2}}\right)^{1/2}$$

so that instead of $Q = 12$ mbar.l/s for 20 bar of N_2, the leak rate would be $Q = 224$ mbar.l/s for 100 bar of H_2. To compensate for that increase and keep the background pressure below $P_{eq}^{(1)} = 3 \times 10^{-3}$ mbar, as when using N_2, the pumping speed should be higher than $R_{eff} = 7.4 \times 10^4$ l/s which is unrealistic as the largest turbo-molecular pumps on the market have maximum pumping speeds of 4000 l/s. Alternatively, one can compute the equilibrium pressure using the same pump but one should notice that H_2 is more difficult to pump than N_2. In fact, heavy gases are easier to pump than light gases; the compression ratio of the turbo-molecular pump goes as $K \propto \exp(\sqrt{M})$ with M the molar mass of the gas, and the pumping speed goes as $S \propto -\ln(K)$ [26, 27], so the lighter the gas, the slower the pumping speed of the turbomolecular pump. This has been the bottleneck for using continuous flows of He or H_2 in LWFA. For example, in our system, the pumping speed of our turbo-molecular pump drops down from 4000 l/s in N_2 to 300 l/s in H_2 at $P = 10^{-1}$ mbar. In practice, this means that for $P_0 = 100$ bar of H_2, the equilibrium pressure would be around $P_{eq}^{(1)} \simeq 0.5$ mbar, which is likely too high for the turbo-molecular pump to sustain. Similar conclusions could be reached for He.

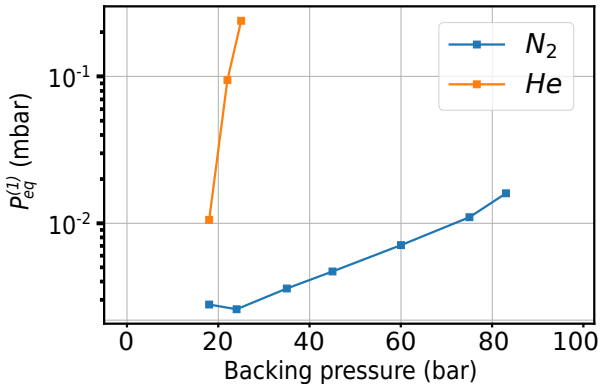

Figure 2. Without differential pumping: equilibrium pressure in the interaction chamber versus backing pressure for a gas nozzle with throat diameter $D^* = 100\,\mu$m. The pumping system is a turbo-molecular pump 4000 l/s.

This has been verified experimentally: we have measured the pressure in the vacuum chamber in which a supersonic nozzle lets out a continuous flow of gas. The vacuum chamber is pumped by a $R_{eff} = 4000$ l/s turbo-molecular pump connected to a primary pump with pumping speed 130 l/s. In Figure 2, we show the variation of the equilibrium pressure versus backing pressure for N_2, and He. The results show very clearly that for He, the equilibrium pressure increases abruptly above $P_{back} = 20$ bar and the pumping system diverges above that, not being able to dispose of the high He flow. This clearly confirms that a specific solution should be implemented for pumping high-pressure ($P > 100$ bar) light gases.

B. Design of the differential pumping system

An alternative solution is to use differential pumping: the gas jet is enclosed in a small vacuum chamber, the differential chamber, that is pumped by a powerful primary pump able to work efficiently at the mbar level with a pumping speed of 360 l/s. The idea is to pump out most of the gas from the small chamber while tolerating a higher equilibrium pressure at the mbar level, $P_{eq}^{(2)} \sim$ mbar within the differential chamber subsystem. Thus, by restricting the leakage from the differential chamber to the main chamber, the pressure can be kept below $P_{eq}^{(1)} < 10^{-3}$ mbar in the main chamber. In this case, the laser propagation is not affected by the residual

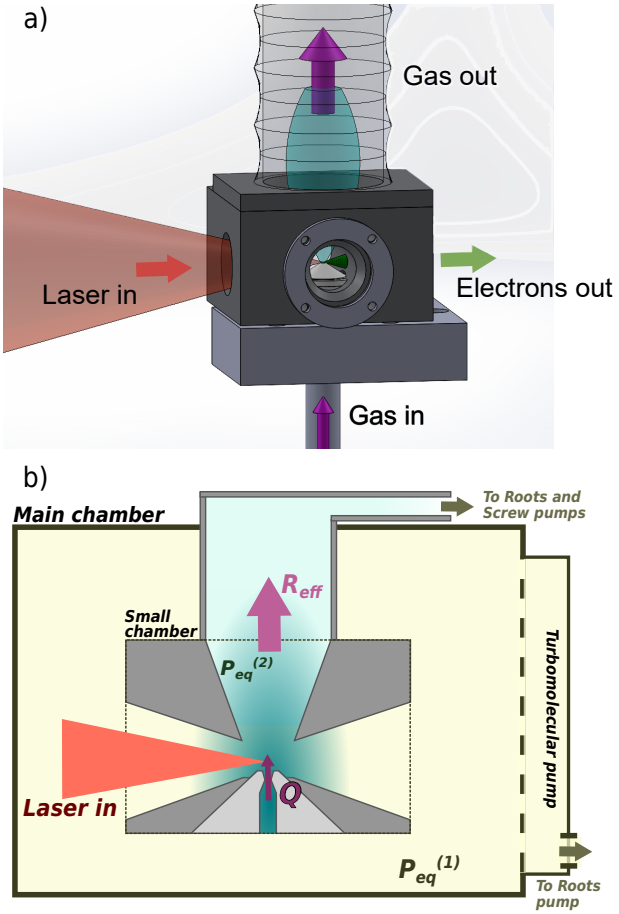

Figure 3. a) Schematic of the differential chamber. b) Conceptual design for differential pumping with a free-flowing high-density gas jet.

gas, provided that the mbar region in the differential chamber is sufficiently short, e.g. millimeter scale. Figure 3 shows a conceptual schematic of the differential scheme that is implemented in the experiment. The laser enters and exits the chamber via two cones that terminate with 1 mm holes for restricting gas leakage. In addition, the "high" density region is limited to 4mm gap in between the two cones to limit its impact on laser propagation.

1D model used to design the differential pumping
Interestingly, the experimental measurement of the gas leak rate Q can be compared to a theoretical estimation using well-known fluid gas dynamics [29]. An estimation of the mass flow rate can be obtained using a 1D isentropic model of the gas flow in the nozzle. For a 1D stationary and turbulent flow, the mass flow rate $\dot{m} = \rho\nu A$ is constant throughout the flow; at the nozzle throat, it reduces to:

$$\dot{m} = \rho^*\nu^*A^* = \gamma^{1/2}\left(\frac{\gamma+1}{2}\right)^{-\frac{\gamma+1}{2(\gamma-1)}}\frac{P_0}{\sqrt{RT_0}}A^* \qquad (3)$$

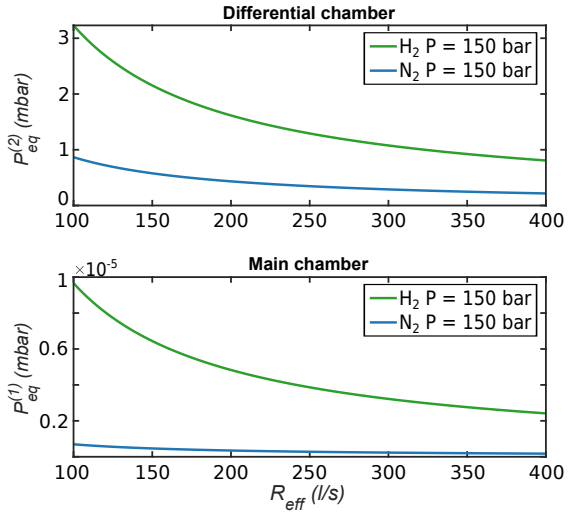

Figure 4. Equilibrium pressure in the chambers as a function of effective pumping speed of the differential chamber R_{eff} for a H_2 gas leak of 320 mbar.l/s, corresponding to a backing pressure of 150 bar and a nozzle with $D^* = 60\,\mu$m. The pumping speed for the main chamber is assumed to be 4000 l/s and the two holes for the differential pumping are 1 mm in diameter.

where ρ^*, ν^* and A^* are respectively the mass density, fluid velocity, and the surface at the nozzle throat, P_0 and T_0 are the pressure and temperature in the reservoir. Note that here, subscript 0 refers to the reservoir, i.e. the stagnation volume where the fluid velocity is $\nu_0 = 0$. The leak rate in mbar.l/s can then be obtained from $Q = PdV/dt = k_BT\frac{dN}{dt}$ which can eventually be written as:

$$Q = \dot{m}RT \qquad (4)$$

with $R = R_0/M$, $R_0 = 8.314\,$J/mol/K is the perfect gas constant and M is the molar mass of the fluid. Taking $P_{back} = P_0 = 20\,$bar and $T = T_0 = 300\,$K for a nozzle with $D = 50\,\mu$m, we obtain $Q = 8\,$mbar·l/s, which is close to the experimental value found earlier ($Q_{exp} = 12\,$mbar·l/s). The discrepancy might be due to the fact that the actual throat diameter is not known precisely and deviates from the generic requested value. In any case, this analysis validates the fact that this simple model can be used for designing the pumping system as it provides a pressure estimate that matches with the experimental measurement within a factor of two.
Using this model, it is straightforward to determine $P_{eq}^{(1)}$ and $P_{eq}^{(2)}$, respectively the equilibrium pressures in the experimental and differential chambers, that are reached as a function of the pumping speed R_{eff} used for pumping the differential chamber. Figure 4 shows the results for a backing pressure of $P = 150\,$bar in a nozzle with throat diameter $D^* = 60\,\mu$m. It is clear that the effective pumping speed needs to be larger than $R_{eff} > 100\,$l/s to

maintain the pressure in the differential chamber at the mbar level. When this condition is fulfilled, these estimations confirm that the equilibrium pressure in the main chamber remains at the level $P_{eq}^{(1)} \sim 10^{-5}$ mbar, when the turbo-molecular pump is running at 4000 l/s. Here, we use the concept of effective pumping speed R_{eff}, where R_{eff} is usually smaller than the nominal pumping speed R_{nom} due to the finite conductance of the various elements of the pumping system (tubes, bellows, etc...) and also because the pumping speed varies with the operating pressure. This has to be carefully taken into account when designing the pumping system.
Once the differential pumping system had been set up, we measured the variation of the equilibrium pressure versus backing pressure for N_2 and H_2. Figure 5 shows the measurements: with the differential pumping apparatus, the pressure in the main chamber $P_{eq}^{(1)}$ remains below 3×10^{-4} mbar, even with a backing pressure of 140 bar of H_2 in the gas jet.

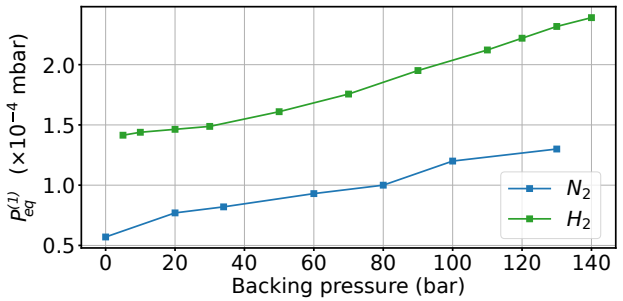

Figure 5. With differential pumping: equilibrium pressure in the interaction chamber versus backing pressure for a gas nozzle with throat diameter $D^* = 60\,\mu$m. The differential chamber is now pumped by a primary pump of 360 l/s.

III. NUMERICAL SIMULATIONS

A. Fluid dynamics simulations

In order to obtain more accurate estimates of the gas flow in the nozzle and the differential chamber, we have performed numerical simulations using the computational fluid dynamics software ANSYS Fluent. Simulations are performed using molecular hydrogen modeled by the Aungier-Redlich-Kwong real gas equation. 3D geometry is used. The results are shown in figure 6 for a H_2 backing pressure of $P_{back} = 100$ bar and a nozzle throat of $D^* = 60\,\mu$m. In the simulations, the boundary conditions at the entrance of the cones and the pumping outlet are taken to be $P = 0$. The simulation results shown in Figure 6a confirm that the pressure remains at the mbar level in the differential chamber, away from the region where the high-density jet is present. Figure 6b shows a dramatic decrease of the density by three orders of magnitude in the gap region between the two cones. The density then steadily decreases along the cone which is favorable for coupling the intense laser into the high-density gas jet without prior interaction. Thus, the gas remains well-confined within the differential chamber, but there is still some stagnation observed about 1 cm before the gas jet, potentially impacting laser performance.

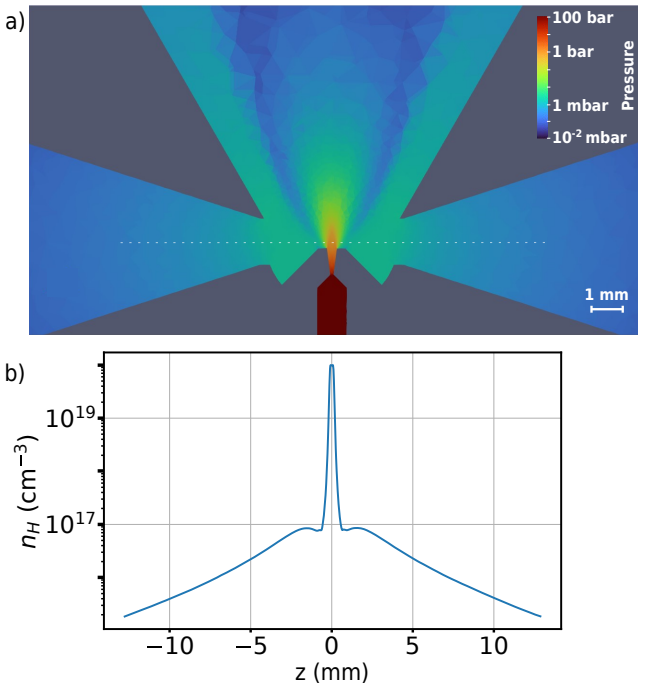

Figure 6. a) Results of CFD simulations showing the pressure in the volume of the differential chamber. b) Lineout of the molecular density along the laser axis.

B. Propagation of the laser pulse up to the gas jet

To evaluate whether the stagnating gas affects laser propagation, we performed simulations of the propagation of the laser pulse from the parabola (at $z = -10$ cm) to the jet (at $z = -200\,\mu$m) using an optical propagation code. The simulations were conducted using three gases : H, He and N in order to assess the potential impact of different gases on the laser pulse. The propagation of the laser through an initially neutral gas was modeled using the open-source library "Axiprop" [30]. This library uses various optical propagators, depending on the specific conditions (gas or vacuum for instance) and concatenate them to handle more complex scenarios. For our study, the paraxial propagator was used for vacuum propagation from the parabola ($z = -10$ cm) to the point where the gas density becomes non-negligible ($z = -10$ mm), as it handles drastic changes in beam size [31]. For the region with gas ($z = -10$ mm to $z = -200\,\mu$m), a non-paraxial propagator was applied, following the method

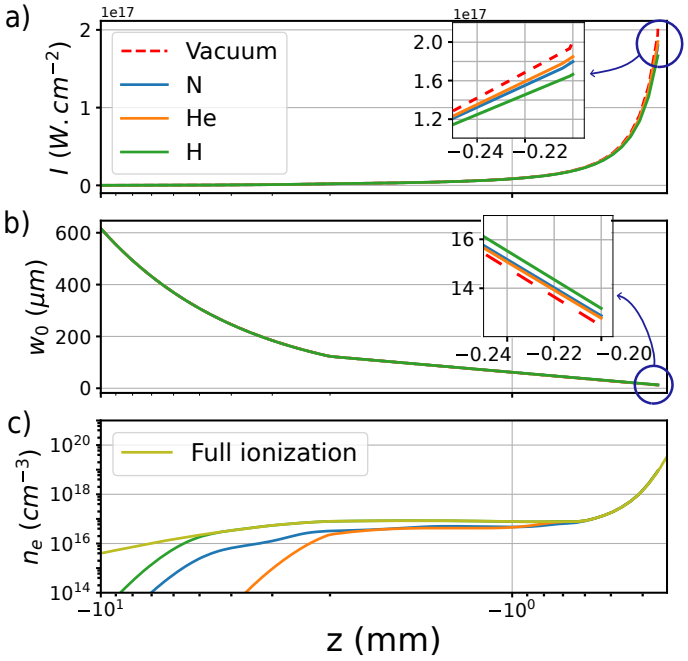

Figure 7. Evolution of the laser parameters as it propagates through the gas profile from $z = -10$ mm to $z = -200\,\mu$m. a) Evolution of the laser intensity I in N, He and H. b) Evolution of the waist of the pulse w_0 in the three gases. c) Electron density along the propagation in the three gases and the target electron density (corresponding to fully ionized He or H gas, and up to the 5^{th} in N gas).

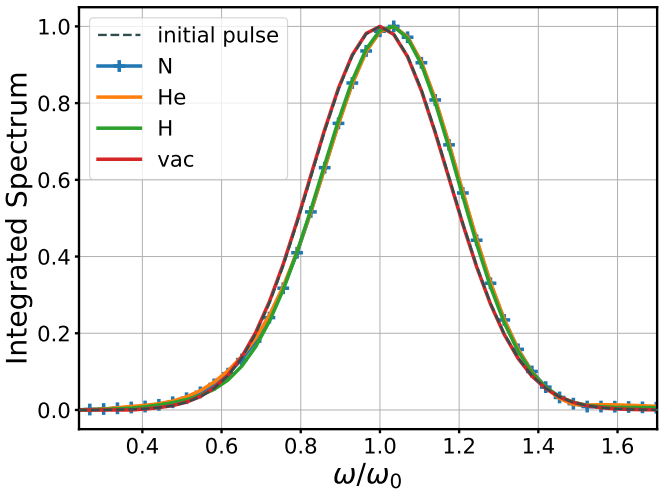

Figure 8. Spectral evolution of the laser pulse after propagation in vacuum, and initially neutral N, He and H gases.

in [32]. Both propagators were implemented using Hankel transforms to account for cylindrical symmetry, as described in [32]. In the gas region, grid sizes were set to $\Delta z = 5.0\,\mu$m for He and N, $\Delta z = 4\,\mu$m for H, and $\Delta r = 0.64\,\mu$m.

Ionization of the gas is simulated using the ADK model [33, 34]. Special care was taken to accurately model ionization, as it is crucial for explaining our experimental results. To model the propagation of the laser in the gas/plasma, the solver that propagates the field within the plasma is similar to the one described by Couairon et al. in [35].

We used the gas density profile obtained with Fluent for N, renormalized so that the peak electron density reaches $n_e = 2 \times 10^{20}\,\text{cm}^{-3}$ after ionization in all three gases. This adjustment considers that N contributes 5 electrons, He contributes 2, and H contributes 1, allowing us to simulate laser propagation at the same electron density for different gases. The laser parameters were kept constant for each case: a duration of 4.2 fs (FWHM), energy of 2.7 mJ, and a focal spot size of 4.5 µm (FWHM), matching our experimental parameters.

Figure 7 illustrates the evolution of the waist (w_0) and laser intensity (I) along the propagation through the density profiles of N, He, and H gases, with vacuum included for reference. The first observation is that the intensity and beam size remain almost identical in both vacuum and gas. The effect of residual gas is negligible and only becomes noticeable at the entrance of the gas jet, where the density inevitably rises, perturbing the laser pulse. Figure 7a shows the evolution of I, where the laser intensity slightly decreases when propagating through gas compared to vacuum, with the largest reduction observed in H (around 20%) and smaller drops of about 10% in N and He. Figure 7b highlights the beam waist (w_0) increasing due to ionization-induced defocusing. The beam size increases by about 7% in H, compared to 5% in N and 4% in He, relative to vacuum. As depicted in Figure 7c, H fully ionizes much earlier than He and N, at around $z = -4.4$ mm, while the others reach full ionization closer to $z = -700\,\mu$m. This difference explains why the laser pulse is slightly more degraded after propagating through H compared to N or He.

Also, the interaction of the pulse with all three gases shifts the spectrum towards the blue. Figure 8 shows the spectrum of the initial pulse and of the pulse at the end of the simulations, integrated over the radial axis, after propagating through vacuum, N, He, or H. When propagating through the three gases, the spectrum shifts slightly to higher frequencies, with a maximum normalized frequency shift of $\omega_{0,\text{max}}/\omega_0 = 1.02$. The laser pulse behaves similarly in all three gases, with no significant differences regarding the final spectrum.

The stagnating gas has a minimal impact on laser propagation. While the interaction of the laser pulse with the gases results in a slight reduction in intensity, some increase in beam size, and a minor blueshift in the spectrum, these changes are negligible. The effects are slightly more pronounced in H due to its lower ionization threshold and the fact that it fully ionizes significantly earlier than He and N.

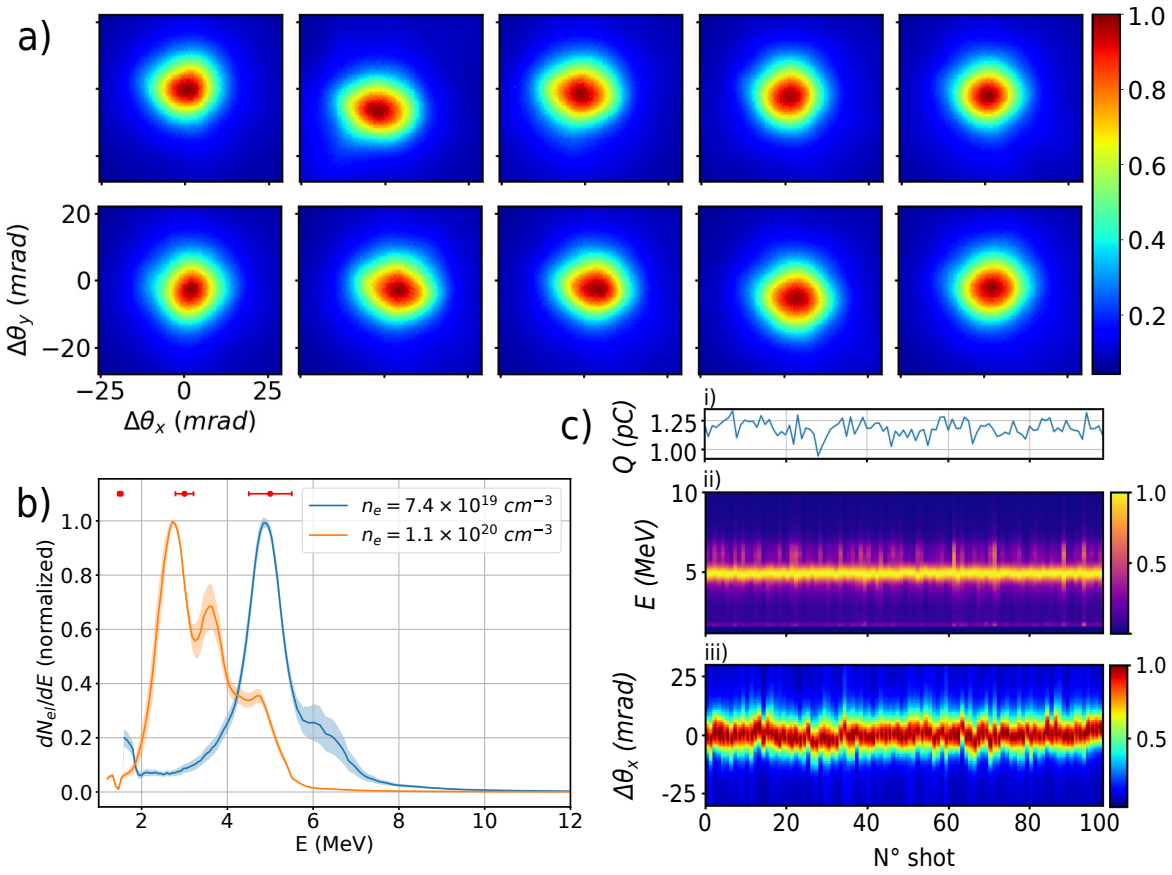

Figure 9. Experimental results obtained in a H_2 (doped N_2) plasma. (a) Single-shot beam profile samples obtained over 10 consecutive shots with $n_e = 1.1 \times 10^{20}\,\mathrm{cm}^{-3}$. (b) Electron spectra. The thickness of the lines corresponds to the RMS fluctuations of the spectrum. (c) Stability over a 100 shots with $n_e = 7.4 \times 10^{19}\,\mathrm{cm}^{-3}$. (i) Charge, (ii) spectra and (iii) beam profile in the x direction, for each shot a slice of 3 pixels around the centroid is shown.

IV. IMPLEMENTATION OF THE DIFFERENTIAL PUMPING APPARATUS : EXPERIMENTAL RESULTS

After designing and simulating this system, we implemented it in our experimental setup to test it in situ, aiming to explore the performance potential of LWFA at 1kHz with the differential pumping system.

A. Experimental set-up

The experimental setup is identical to that described in detail in [28]. The principal information is summarized below. The laser wakefield accelerator is driven by a kHz laser that delivers 4 fs pulses at FWHM with 2.7 mJ on-target energy [36, 37]. The pulses are focused by a 100 mm off-axis parabola down to a 4.5 µm spot at FWHM, reaching a peak intensity in vacuum $I = 1.8 \times 10^{18}\,\mathrm{W \cdot cm^{-2}}$. The laser is focused at a distance of 150 µm from the exit of a continuously flowing supersonic-shocked gas jet with a 180 µm exit diameter [38, 39]. Density characterization is performed with N_2 gas, as in [28, 40] using a quadriwave lateral shearing interferometer (SID4-HR, Phasics, [41, 42]). The density that we refer to in this paper corresponds to the density 150 µm above the nozzle exit.

Specifically, we used shocked gas jets and Hydrogen doped with 2% of Nitrogen. Shocked jets helped confine the electron-trapping region, resulting in electron beams with reduced energy spreads and improved stability [43–46]. Additionally, shock-assisted ionization injection demonstrated an increase in trapped charge compared to pure shock injection while maintaining excellent stability [47].

The electron beam charge, spatial profile, and beam pointing are measured using a calibrated YAG screen imaged onto a 14 bits CCD camera. The electron energy spectrum is measured onto the same YAG screen, by inserting a motorized magnetic spectrometer in the beam, which relies on a set of permanent magnetic dipoles creating a magnetic field of 0.12 T on a 20 mm length. Each

image presented here was obtained by acquiring data over 1 ms (so each image corresponds to a single shot). For each plasma density studied, a series of 100 acquisitions is taken. Statistics over electron beam parameters are then obtained by averaging over the acquisition series, and the uncertainties represent the RMS deviation from the mean value.

B. Results

For each measurement, we optimized the laser pulse duration and focal position. We explored densities ranging from $n_e = 7.4 \times 10^{19}\text{cm}^{-3}$ to $n_e = 1.2 \times 10^{20}\text{cm}^{-3}$. Figure 9a shows a typical electron beam profile at the higher density of $n_e = 1.2 \times 10^{20}, \text{cm}^{-3}$. The beam exhibits a quasi-circular shape with minimal divergence, with very good stability shot to shot as shown in Table I. Figure 9b shows the corresponding electron spectra for two different densities, averaged over 100 shots. The thickness of the lines corresponds to the RMS fluctuations in the dataset. Both spectra reveal low fluctuations, with well-defined energy peaks, confirming the consistent beam quality. The stability of the beam is further demonstrated in Figure 9c, where we present 100 consecutive single-shot acquisitions. The low variance in beam parameters such as charge, divergence, and energy indicates the high level of stability achieved with this setup. Table I summarizes the relative fluctuations of key beam parameters for the two plasma densities. Notably, the beam-pointing fluctuations remain below 2.3 mrad RMS, with charge fluctuations less than 7%, and energy fluctuations as low as 2% shot-to-shot, confirming excellent beam stability throughout the experiment.

	$\mathbf{H_2N_2}$	
n_e (cm^{-3})	7.4×10^{19}	1.1×10^{20}
Point. stab. x	1.46 mrad rms	1.04 mrad rms
Point. stab. y	1.97 mrad rms	2.26 mrad rms
Q	1.2 pC (±6.0 % rms)	3.5 pC (±6.7 % rms)
E_{mean}	5.02 MeV (±2.4 % rms)	3.3 MeV (±1.8 % rms)
E_{spread}	0.99 MeV (±26 % rms)	1.44 MeV (±6.9 % rms)
θ_x	13.0 mrad (±10 % rms)	18.2 mrad (±13 % rms)
θ_y	12.1 mrad (±14 % rms)	16.2 mrad (±11 % rms)

Table I. Stability of the beam : RMS fluctuations of the key beam parameters.

V. CONCLUSION

In this paper, we introduced a novel apparatus that combines high-pressure gas jets with a differential pumping system, enabling the continuous operation of a kHz laser-wakefield accelerator utilizing hydrogen plasma generated from a free-flowing gas jet.
The theoretical calculations demonstrated the importance of this system in meeting operational requirements and guided the design process. The chamber pressure was successfully maintained below 3×10^{-4} mbar, even with a backing pressure of up to 140 bar of hydrogen in the 180 µm aperture gas jet, confirming the effectiveness of this vacuum system. Then, fluid simulations demonstrated that the gas behavior within the chamber does not adversely affect laser pulse propagation.
Finally, we conducted laser wakefield acceleration experiments to test the efficacy of the differential pumping setup, yielding highly stable and well-defined electron beams. This accomplishment represents the first continuous operation at kHz repetition rates with hydrogen, thereby marking a significant advancement in kHz LWFA using light gases.

ACKNOWLEDGMENTS

This project has received funding from the European Union's Horizon 2020 research and innovation program under grant agreement JRA PRISE no. 871124 Laserlab-Europe and IFAST under Grant Agreement No 101004730. This project was also funded by the Agence Nationale de la Recherche under Contract No. ANR-20-CE92-0043-01, and benefited from the support of Institut Pierre Lamoure via the chair "Accélération laser-plasma haute cadence".
This work has benefited from a grant managed by the Agence Nationale de la Recherche (ANR), as part of the program 'Investissements d'Avenir' under the reference (ANR-18-EURE-0014).
Financial support from the Région Ile-de-France (under Contract No. SESAME-2012-ATTOLITE) and the Extreme Light Infrastructure-Hungary Non-Profit Ltd (under Contract No. NLO3.6LOA) is gratefully acknowledged. We also acknowledge Laserlab-Europe, Grant No. H2020 EC-GA 654148 and the Lithuanian Research Council under Grant agreement No. S-MIP-21-3..

DATA AVAILABILITY

The data that support the findings of this study are available from the corresponding author upon reasonable request.

[1] T. Tajima and J. M. Dawson, Laser Electron Accelerator, Phys. Rev. Lett. **43**, 267 (1979).

[2] S. Semushin and V. Malka, High density gas jet nozzle design for laser target production, Review of Scientific Instruments **72**, 2961 (2001).

[3] K. Schmid and L. Veisz, Supersonic gas jets for laser-plasma experiments, Review of Scientific Instruments **83**, 053304 (2012).

[4] J. Osterhoff, A. Popp, Z. Major, B. Marx, T. P. Rowlands-Rees, M. Fuchs, M. Geissler, R. Hörlein, B. Hidding, S. Becker, E. A. Peralta, U. Schramm, F. Grüner, D. Habs, F. Krausz, S. M. Hooker, and S. Karsch, Generation of Stable, Low-Divergence Electron Beams by Laser-Wakefield Acceleration in a Steady-State-Flow Gas Cell, Phys. Rev. Lett. **101**, 085002 (2008).

[5] M. Kirchen, S. Jalas, P. Messner, P. Winkler, T. Eichner, L. Hübner, T. Hülsenbusch, L. Jeppe, T. Parikh, M. Schnepp, and A. R. Maier, Optimal Beam Loading in a Laser-Plasma Accelerator, Phys. Rev. Lett. **126**, 174801 (2021).

[6] P. Drobniak, E. Baynard, K. Cassou, D. Douillet, J. Demailly, A. Gonnin, G. Iaquaniello, G. Kane, S. Kazamias, N. Lericheux, B. Lucas, B. Mercier, Y. Peinaud, and M. Pittman, Two-chamber gas target for laser-plasma accelerator electron source (2023).

[7] W. P. Leemans, B. Nagler, A. J. Gonsalves, C. Tóth, K. Nakamura, C. G. R. Geddes, E. Esarey, C. B. Schroeder, and S. M. Hooker, GeV electron beams from a centimetre-scale accelerator, Nature Phys **2**, 696 (2006).

[8] J. Ulbricht, G. Clausnitzer, and G. Graw, High density windowless gas target, Nuclear Instruments and Methods **102**, 93 (1972).

[9] G. Bittner, W. Kretschmer, and W. Schuster, A windowless high-density gas target for nuclear scattering experiments, Nuclear Instruments and Methods **167**, 1 (1979).

[10] M. Treichel, R. Isenbügel, and N. Marquardt, A differentially pumped supersonic jet gas target for low-energy nuclear reaction experiments, Nuclear Instruments and Methods in Physics Research **212**, 101 (1983).

[11] D. Shapira, J. Ford, R. Novotny, B. Shivakumar, R. Parks, and S. Thornton, The HHIRF supersonic gas jet target facility, Nuclear Instruments and Methods in Physics Research Section A: Accelerators, Spectrometers, Detectors and Associated Equipment **228**, 259 (1985).

[12] S. Bohlen, J. C. Wood, T. Brümmer, F. Grüner, C. A. Lindstrøm, M. Meisel, T. Staufer, R. D'Arcy, K. Põder, and J. Osterhoff, Stability of ionization-injection-based laser-plasma accelerators, Phys. Rev. Accel. Beams **25**, 031301 (2022).

[13] S. P. D. Mangles, C. D. Murphy, Z. Najmudin, A. G. R. Thomas, J. L. Collier, A. E. Dangor, E. J. Divall, P. S. Foster, J. G. Gallacher, C. J. Hooker, D. A. Jaroszynski, A. J. Langley, W. B. Mori, P. A. Norreys, F. S. Tsung, R. Viskup, B. R. Walton, and K. Krushelnick, Monoenergetic beams of relativistic electrons from intense laser–plasma interactions, Nature **431**, 535 (2004).

[14] C. G. R. Geddes, C. Toth, J. van Tilborg, E. Esarey, C. B. Schroeder, D. Bruhwiler, C. Nieter, J. Cary, and W. P. Leemans, High-quality electron beams from a laser wakefield accelerator using plasma-channel guiding, Nature **431**, 538 (2004).

[15] J. Faure, Y. Glinec, A. Pukhov, S. Kiselev, S. Gordienko, E. Lefebvre, J.-P. Rousseau, F. Burgy, and V. Malka, A laser–plasma accelerator producing monoenergetic electron beams, Nature **431**, 541 (2004).

[16] H. T. Kim, V. B. Pathak, K. Hong Pae, A. Lifschitz, F. Sylla, J. H. Shin, C. Hojbota, S. K. Lee, J. H. Sung, H. W. Lee, E. Guillaume, C. Thaury, K. Nakajima, J. Vieira, L. O. Silva, V. Malka, and C. H. Nam, Stable multi-GeV electron accelerator driven by waveform-controlled PW laser pulses, Sci Rep **7**, 10203 (2017).

[17] K. Oubrerie, A. Leblanc, O. Kononenko, R. Lahaye, I. A. Andriyash, J. Gautier, J.-P. Goddet, L. Martelli, A. Tafzi, K. T. Phuoc, S. Smartsev, and C. Thaury, Controlled acceleration of GeV electron beams in an all-optical plasma waveguide, Light: Science and Applications **11**, 180 (2022).

[18] B. Miao, J. Shrock, L. Feder, R. Hollinger, J. Morrison, R. Nedbailo, A. Picksley, H. Song, S. Wang, J. Rocca, and H. Milchberg, Multi-GeV Electron Bunches from an All-Optical Laser Wakefield Accelerator, Phys. Rev. X **12**, 031038 (2022).

[19] A. Gonsalves, K. Nakamura, J. Daniels, C. Benedetti, C. Pieronek, T. de Raadt, S. Steinke, J. Bin, S. Bulanov, J. van Tilborg, C. Geddes, C. Schroeder, C. Tóth, E. Esarey, K. Swanson, L. Fan-Chiang, G. Bagdasarov, N. Bobrova, V. Gasilov, G. Korn, P. Sasorov, and W. Leemans, Petawatt Laser Guiding and Electron Beam Acceleration to 8 GeV in a Laser-Heated Capillary Discharge Waveguide, Phys. Rev. Lett. **122**, 084801 (2019).

[20] J. Faure, D. Gustas, D. Guénot, A. Vernier, F. Böhle, M. Ouillé, S. Haessler, R. Lopez-Martens, and A. Lifschitz, A review of recent progress on laser-plasma acceleration at kHz repetition rate, Plasma Phys. Control. Fusion **61**, 014012 (2018).

[21] D. Guénot, D. Gustas, A. Vernier, B. Beaurepaire, F. Böhle, M. Bocoum, M. Lozano, A. Jullien, R. Lopez-Martens, A. Lifschitz, and J. Faure, Relativistic electron beams driven by kHz single-cycle light pulses, Nature Photon **11**, 293 (2017).

[22] D. Gustas, D. Guénot, A. Vernier, S. Dutt, F. Böhle, R. Lopez-Martens, A. Lifschitz, and J. Faure, High-charge relativistic electron bunches from a kHz laser-plasma accelerator, Phys. Rev. Accel. Beams **21**, 013401 (2018).

[23] F. Salehi, A. J. Goers, G. A. Hine, L. Feder, D. Kuk, B. Miao, D. Woodbury, K. Y. Kim, and H. M. Milchberg, MeV electron acceleration at 1 kHz with <10 mJ laser pulses, Opt. Lett., OL **42**, 215 (2017).

[24] L. Rovige, J. Huijts, I. Andriyash, A. Vernier, V. Tomkus, V. Girdauskas, G. Raciukaitis, J. Dudutis, V. Stankevic, P. Gecys, M. Ouille, Z. Cheng, R. Lopez-Martens, and J. Faure, Demonstration of stable long-term operation of a kilohertz laser-plasma accelerator, Phys. Rev. Accel. Beams **23**, 093401 (2020).

[25] F. Salehi, M. Le, L. Railing, M. Kolesik, and H. Milchberg, Laser-Accelerated, Low-Divergence 15-MeV Quasimonoenergetic Electron Bunches at 1 kHz, Phys. Rev. X **11**, 021055 (2021).

[26] W. Gaede, Die Diffusion der Gase durch Quecksilberdampf bei niederen Drucken und die Diffusionsluft-

pumpe, Annalen der Physik **351**, 357 (1915).
[27] W. Becker, The turbomolecular pump, its design, operation and theory; calculation of the pumping speed for various gases and their dependence on the forepump, Vacuum **16**, 625 (1966).
[28] J. Monzac, S. Smartsev, J. Huijts, L. Rovige, I. A. Andriyash, A. Vernier, V. Tomkus, V. Girdauskas, G. Raciukaitis, M. Mackevičiūtė, V. Stankevic, A. Cavagna, J. Kaur, A. Kalouguine, R. Lopez-Martens, and J. Faure, Optical ionization effects in kHz laser wakefield acceleration with few-cycle pulses (2024).
[29] R. D. Zucker and O. Biblarz, *Fundamentals of Gas Dynamics*, 2nd ed. (John Wiley & Sons Inc, Hoboken, NJ, 2002).
[30] I. Andriyash, hightower8083/axiprop (2024).
[31] J. W. Goodman, *Introduction to Fourier Optics* (Roberts and Company Publishers, 2005).
[32] K. Oubrerie, I. A. Andriyash, R. Lahaye, S. Smartsev, V. Malka, and C. Thaury, Axiparabola: a new tool for high-intensity optics, J. Opt. **24**, 045503 (2022).
[33] M. V. Ammosov, N. B. Delone, and V. P. Krainov, Tunnel ionization of complex atoms and of atomic ions in an alternating electromagnetic field, Soviet Journal of Experimental and Theoretical Physics **64**, 1191 (1986).
[34] S. Augst, D. Strickland, D. D. Meyerhofer, S. L. Chin, and J. H. Eberly, Tunneling ionization of noble gases in a high-intensity laser field, Phys. Rev. Lett. **63**, 2212 (1989).
[35] A. Couairon, E. Brambilla, T. Corti, D. Majus, O. de J. Ramírez-Góngora, and M. Kolesik, Practitioner's guide to laser pulse propagation models and simulation, Eur. Phys. J. Spec. Top. **199**, 5 (2011).
[36] F. Böhle, M. Kretschmar, A. Jullien, M. Kovacs, M. Miranda, R. Romero, H. Crespo, U. Morgner, P. Simon, R. Lopez-Martens, and T. Nagy, Compression of CEP-stable multi-mJ laser pulses down to 4 fs in long hollow fibers, Laser Phys. Lett. **11**, 095401 (2014).
[37] M. Ouillé, A. Vernier, F. Böhle, M. Bocoum, A. Jullien, M. Lozano, J.-P. Rousseau, Z. Cheng, D. Gustas, A. Blumenstein, P. Simon, S. Haessler, J. Faure, T. Nagy, and R. Lopez-Martens, Relativistic-intensity near-single-cycle light waveforms at kHz repetition rate, Light Sci Appl **9**, 47 (2020).
[38] V. Tomkus, V. Girdauskas, J. Dudutis, P. Gečys, V. Stankevič, and G. Račiukaitis, High-density gas capillary nozzles manufactured by hybrid 3D laser machining technique from fused silica, Opt. Express, OE **26**, 27965 (2018).
[39] A. Marcinkevičius, S. Juodkazis, M. Watanabe, M. Miwa, S. Matsuo, H. Misawa, and J. Nishii, Femtosecond laser-assisted three-dimensional microfabrication in silica, Opt. Lett., OL **26**, 277 (2001).
[40] L. Rovige, J. Huijts, A. Vernier, I. Andriyash, F. Sylla, V. Tomkus, V. Girdauskas, G. Raciukaitis, J. Dudutis, V. Stankevic, P. Gecys, and J. Faure, Symmetric and asymmetric shocked gas jets for laser-plasma experiments, Review of Scientific Instruments **92**, 083302 (2021).
[41] J. Primot and L. Sogno, Achromatic three-wave (or more) lateral shearing interferometer, J. Opt. Soc. Am. A, JOSAA **12**, 2679 (1995).
[42] J. Primot and N. Guérineau, Extended Hartmann test based on the pseudoguiding property of a Hartmann mask completed by a phase chessboard, Appl. Opt., AO **39**, 5715 (2000).
[43] S. Bulanov, N. Naumova, F. Pegoraro, and J. Sakai, Particle injection into the wave acceleration phase due to nonlinear wake wave breaking, Phys. Rev. E **58**, R5257 (1998).
[44] H. Suk, N. Barov, J. B. Rosenzweig, and E. Esarey, Plasma Electron Trapping and Acceleration in a Plasma Wake Field Using a Density Transition, Phys. Rev. Lett. **86**, 1011 (2001).
[45] P. Tomassini, M. Galimberti, A. Giulietti, D. Giulietti, L. A. Gizzi, L. Labate, and F. Pegoraro, Production of high-quality electron beams in numerical experiments of laser wakefield acceleration with longitudinal wave breaking, Phys. Rev. ST Accel. Beams **6**, 121301 (2003).
[46] J. U. Kim, N. Hafz, and H. Suk, Electron trapping and acceleration across a parabolic plasma density profile, Phys. Rev. E **69**, 026409 (2004).
[47] C. Thaury, E. Guillaume, A. Lifschitz, K. Ta Phuoc, M. Hansson, G. Grittani, J. Gautier, J. P. Goddet, A. Tafzi, O. Lundh, and V. Malka, Shock assisted ionization injection in laser-plasma accelerators, Scientific Reports **5**, 16310 (2015).